euspen's 26th International Conference & Exhibition, Krakow, PL, June 2026
www.euspen.eu

Modelling of 3D Surface Topography in Micromilling Process with Material Accumulation Effect

Marcin Gołaszewski[1] Bartosz Powałka[1]

[1]*West Pomeranian University of Technology in Szczecin, Poland*

marcin.golaszewski@zut.edu.pl

Abstract
Modelling of 3D surface topography in micromilling processes remains a key challenge in precision manufacturing. Since not all mechanisms have been fully identified, recent research has increasingly focused on advanced modelling approaches that enable the identification of new factors influencing the machining process. In this context, the present study introduces a hybrid model that combines 2D and 3D modules to predict both the machined surface topography and cutting forces. The model accounts for the phenomenon of material accumulation during micromilling and is applicable for feed per tooth values not exceeding the minimum uncut chip thickness. This accumulation phenomenon results from tool rigidity and the incomplete removal of material in the cross-section of the cut layer. To validate the model, grooves were machined using progressive feed per tooth values of 0.1 µm, 0.2 µm, and 0.3 µm with a flat-end micro tool of diameter D = 0.5 mm. The results confirmed that the marks observed on the machined surface are caused by the accumulation mechanism. The proposed model enables accurate estimation of the size of these accumulation marks. Furthermore, the influence of tool stiffness and minimum uncut chip thickness on the accumulation mechanism was analysed in detail.

micromilling; modelling; 3D surface topography; cutting forces; accumulation mechanism

1. Introduction

Milling is a material removal process in which machining is performed by a rotating multi-edge cutting tool. The cutter features cutting edges uniformly distributed around its axis, and the interaction between its rotational motion and the feed motion of the workpiece enables the generation of the machined surface geometry. Milling is therefore suitable for producing a wide range of surface forms and complex shapes.

The increasing demand for miniaturized components with characteristic dimensions ranging from several tens of micrometers to a few millimeters has stimulated the rapid development of micromachining technologies, with micromilling playing a particularly important role. Micromilling extends the conventional milling process to the microscale, where material removal is governed not only by geometric cutting parameters but also by the uncut chip thickness and microscale-specific material removal mechanisms [1].

According to classical machining theory, the resulting surface topography is primarily determined by the kinematic-geometric projection of the tool tip onto the workpiece, which depends on parameters such as feed per tooth, nominal tool diameter, or corner radius.

However, in micromilling this theoretical description exhibits limited predictive accuracy. The final surface topography is strongly influenced by additional factors. Most often, the literature considers factors such as geometrical errors of machining system, tool wear, vibrations, and other specific phenomena characterizing the micromilling process.

Cutting forces generated during milling have a significant influence on the formation of machined surface topography, as they lead to deflections of the tool tip [2]. These forces induce periodic elastic deformations of the tool and the workpiece, which may result in surface location errors and, in certain cases, contribute directly to surface roughness.

The special case is processing when the frequencies of force variations exceed the frequency corresponding to the feed per revolution [3]. In addition, vibrations and loss of process stability, manifested by the occurrence of chatter, constitute highly undesirable phenomena that affect surface quality. The formation of high-amplitude chatter marks on milled surfaces is influenced by aliasing and pseudo-moiré effects [4]. Furthermore, instantaneous tool tip deflections can induce milling vibrations, which are subsequently transferred onto the machined surface, leading to further deterioration of the surface finish [5].

When the cutting thickness reach level below the minimum chip thickness h_{min}, material removal does not occur through conventional chip formation; instead, the workpiece material undergoes predominantly elastic-plastic deformation, commonly referred to as ploughing. Once the cutting thickness reaches or exceeds h_{min}, the contribution of ploughing is significantly reduced and stable chip formation is established [6,7]. This transition in the material removal mechanism gives rise to the so-called size effect. This behavior is associated with the elevated shear flow stress resulting from the reduced dimensions of the cutting zone [8]. Consequently, the size effect has a substantial influence on both cutting forces and the resulting surface quality of machined components.

This paper presents a micro-machining model for both, the machined surface and the micromilling forces, including the mechanism of chip accumulation. This mechanism plays a key role in machining with low rates of feed per tooth.

2. Micromilling model

In this study, a novel 3D surface topography model dedicated to micromilling and based on a 2D solver is proposed. The developed model describes the trochoidal trajectory of the tool tip as well as the material accumulation mechanism [9]. Furthermore, the modelling framework accounts for instantaneous radial tool tip displacement induced by cutting forces.

The proposed surface topography model integrates a 2D HMT-based approach (Homogenous Matrix Transformation) with a 3D Z-map method within dedicated computational modules. The 2D HMT-based model is employed to determine the instantaneous positions of the cutting edges, which are required to evaluate the instantaneous area of cut and, consequently, to calculate the cutting force components. Additionally, the 2D HMT-based model incorporates both the material accumulation mechanism and radial tool tip displacements. The 3D Z-map model is subsequently used to generate the machined surface topography. It employs the geometrical outlines of successive cutting edges obtained from the 2D HMT-based model by transforming the cutting edges motion into a three-dimensional representation. An overview of the proposed surface topography modelling procedure is presented in Figure 1.

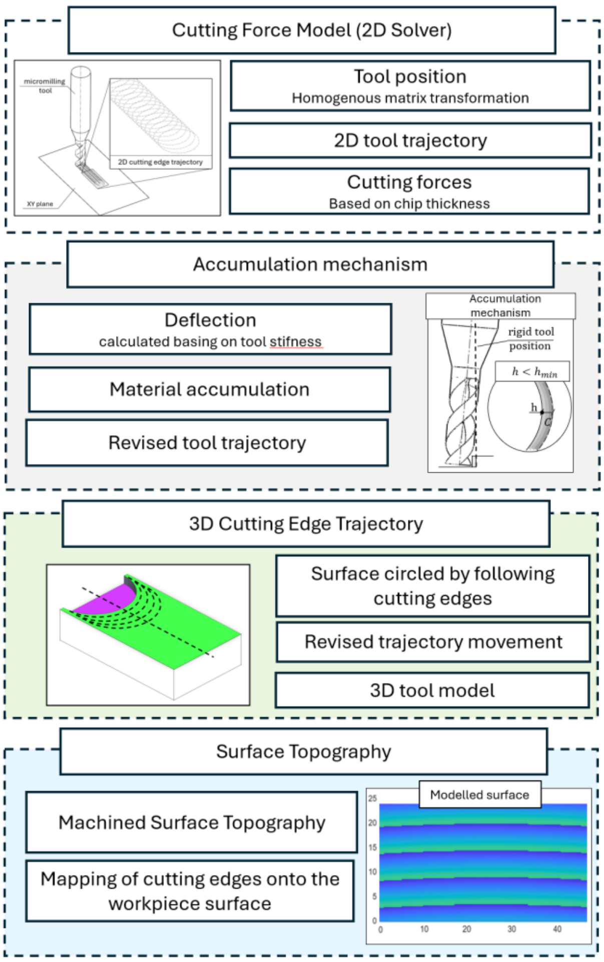

Figure 1. Overview of the proposed modelling procedure

2.1. 2D HMT-based model

In the 2D HMT-based approach, the cutting edge is represented as a point in a two-dimensional plane. This representation enables a reduction in computational time. The employed algorithms require iterative updates of the cutting edge position according to the tool motion as well as accumulation-based tool deflection therefore, reducing the complexity of algorithms is reasonable. The positions of the cutting edges are mutually related and defined with respect to the tool center, which coincides with the rotation axis. Each cutting edge is described by its coordinates in the X and Y axes. The position of cutting edge C is defined as shown in Eq. (1).

The position of a cutting edge at a given time t is determined using a homogeneous matrix transformation that incorporates both translational and rotational components. The angular position of the cutting edge, denoted as φ(t), together with the feed ratio, constitutes the key parameters of this transformation. All changes in tool position resulting from tool deflection and the accumulation mechanism are introduced into the model using homogeneous matrix transformations. The position of the cutting edge at a single time instant t is described by Eq. (2). The motion-related matrices are denoted as $R_z(t)$ for rotation and $T_x(t)$ for feed, while the accumulation-based tool deflection is represented by the matrix $T_r(t)$.

$$C = \begin{bmatrix} x|_{t=0} \\ y|_{t=0} \end{bmatrix} \tag{1}$$

$$C^T = C^T|_{t=0} \cdot T_r(t) \cdot R_z(t) \cdot T_x(t) \tag{2}$$

To determine the trajectory traced by a cutting edge during a single tool revolution, the cutting edge position is evaluated at discrete time intervals. Between two consecutive instants, t and t + Δt, the cutting edge undergoes rotation about the tool axis and a simultaneous displacement of the tool center. This combined motion generates a trochoidal trajectory. During a single tool pass, the rotating cutting edge produces curved trochoidal lines corresponding to the removed material. The material removal region is bounded by the trochoidal lines formed during successive revolutions. Notably, each marked area is associated with an individual cutting edge rather than with the entire tool. Consequently, the model constructs as many surface segments as there are cutting edges. The trochoidal trajectories traced by all cutting edges collectively define the overall material removal process.

2.2. Model of micromilling cutting forces

In order to estimate the instantaneous cutting forces and tool tip displacements, two coordinate systems, XYZ and TRA, are adopted in the modeling framework. In the XYZ coordinate system, the cutting forces measured by the dynamometer are defined. In this system, the Z-axis coincides with the tool axis, the X-axis corresponds to the feed direction, and the Y-axis is defined by the right-hand rule based on the X and Z axes. The TRA coordinate system is a tool-fixed reference frame, with its origin located at the tool tip. In this system, the R-axis represents the radial direction, the A-axis coincides with the tool axis, and the T-axis is defined by the orientation of the A and R axes. The TRA coordinate system rotates together with the tool during spindle rotation.

Assuming perfect rigidity of the system in the axial direction, the force components along the A and Z axes are not considered. The transformation of the cutting force components from the TRA system to the XYZ system is described by Eqs. (3) and (4). The detailed procedure for determining the cutting force components is provided in previous studies [10].

$$F_X = F_T \cdot \cos\varphi(t) + F_R \cdot \sin\varphi(t) \tag{3}$$

$$F_Y = -F_T \cdot \sin\varphi(t) + F_R \cdot \cos\varphi(t) \tag{4}$$

The radial tool deflection Δr is determined using an iterative algorithm. In each iteration, an elementary deflection dr is introduced in the direction that drives the system toward mechanical equilibrium. After applying the elementary deflection, a new tool position is calculated. This positional change results in a reduction of the uncut chip thickness. Based on the updated tool position, new cutting force components in the TRA coordinate system are evaluated. Subsequently, the elastic forces acting on the tool are recalculated. If the equilibrium conditions are not satisfied, the algorithm proceeds to the next iteration.

The elastic force in the j-th iteration, denoted as F_{krj}, is calculated using Eq. (5), where F_{Rm} and F_{krm} represent the force values obtained in the m-th iteration. The iterative procedure continues until an equilibrium state is reached. The tool deflection corresponding to the equilibrium state obtained in the j-th iteration is then determined using Eq. (6).

$$F_{krj} = k_r \cdot \sum_{m=1}^{j-1} \frac{(F_{Rm} - F_{krm})}{|F_{Rm} - F_{krm}|} \cdot dr \tag{5}$$

$$\Delta r = \sum_{m=1}^{j} \frac{(F_{Rm} - F_{krm})}{|F_{Rm} - F_{krm}|} \cdot dr \tag{6}$$

Taking into account the determined radial deflection Δr, the instantaneous position of the cutting edge is updated. Material that would be removed by a perfectly rigid cutting edge during the current pass is transferred to the subsequent pass. Furthermore, it is assumed that when the uncut chip thickness does not exceed a minimum value h_{min}, the material is not removed, despite the presence of non-zero cutting forces. In such a case, the unremoved material is added to the uncut chip thickness in the next cutting edge pass. This phenomenon is referred to as the material accumulation effect. The material continues to accumulate until the cumulative instantaneous uncut chip thickness exceeds the h_{min} value. Once this condition is satisfied, the material is removed and the accumulation cycle restarts. A schematic illustration of the method of uncut chip thickness determination is presented in the figure 2.

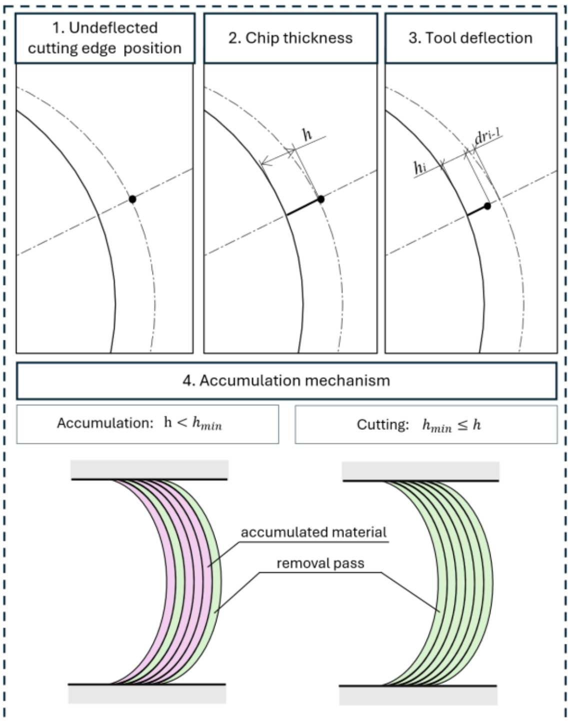

Figure 2. Overview of the proposed modelling procedure

2.3 3D Z-map transformation

The tool trajectory determined in the 2D HMT-based module accounts for both radial tool deflection and the material accumulation mechanism. In this form, the trajectories of the cutting edges can be directly adapted for three-dimensional surface representation.

In the first step, a three-dimensional model of the cutting tool is constructed. The tool is represented as a point cloud, with the cutting edge geometry obtained by determining the intersection of the tool body with a plane inclined by the helix angle λ. The modeled cutting edge is divided into three distinct regions: the face cutting edge, the cylindrical cutting edge, and the corner radius cutting edge. Each region is modeled separately in order to accurately capture the local geometry of the tool body. This segmentation enables a precise representation of the cutting edge geometry and ensures reliable simulation of tool–workpiece interaction.

The workpiece model is limited to the representation of the machined surface only. Similar to the tool model, the workpiece is described using a point cloud format. The grid of workpiece points is based on a rectangular mesh, which is assumed to be the master mesh inherited by the machined surface topography model.

The surface generated by the cutting edge is constructed from its successive positions, forming a radial mesh without predefined nodes. The locations of these nodes are determined dynamically based on the instantaneous position of the cutting edge. Consequently, the mesh of the traced surface differs from the predefined workpiece mesh. To enable accurate surface modeling within the workpiece domain, the nodes of the traced surface mesh are dynamically adjusted. As a result, the cutting edge surface mesh is interpolated to match the predefined workpiece mesh.

Once the surface generated by the cutting edge is described on the same mesh as the workpiece, the Z-map model is applied. The Z-map approach is based on comparing the geometry values at corresponding nodes of two meshes: a modified mesh and a modifying mesh. In the present case, the workpiece material constitutes the modified geometry, while the surface generated by the cutting edge represents the modifying geometry. If the geometry value at a node of the modified mesh is greater than the corresponding value of the modifying mesh, the modified geometry is updated to the value of the modifying geometry. Otherwise, the modified geometry retains its original value.

2.4. Experimental results and discussion

Micromilling experiments were conducted on AISI 1045 carbon steel. Cutting tests were conducted with a radial depth of cut a_e =20 µm and a cutting speed v_c = 47 m/min. The feed per tooth values were set below the minimum uncut chip thickness. For the 2FESM005-010-04 tool with a diameter D = 0.5 mm, the minimum uncut chip thickness was determined as h_{min} = 0.64 µm. This value was estimated based on the cutting edge radius r_n = 3.2 µm. The experiments were carried out for feed per tooth values of f_{z1} = 0.1 µm, f_{z2} = 0.2 µm and f_{z3} = 0.3 µm.

The radial stiffness of the tool was determined experimentally. The displacement was induced using a rigid steel block attached to the moving machine table. The displacement was applied incrementally in steps of 1 µm. The tool tip was supported against a movable block with a cylindrical surface. The resulting radial stiffness was determined as k_r = 0.15 N/µm.

On the machined surface, marks resembling feed marks were observed; however, their spacing did not correspond to the nominal feed per tooth. In order to explain the mechanism responsible for their formation, the algorithm described in the previous section, incorporating the accumulation phenomenon, was employed. The spacing between consecutive accumulation marks was approximately 5.6 μm, which is significantly greater than the applied feed per tooth.

The accumulation phenomenon, consisting in the gradual build-up of material until the minimum uncut chip thickness is exceeded, is particularly significant for feed values far below h_{min}. This mechanism makes it possible to explain the occurrence of surface marks whose spacing is a multiple of the nominal feed per tooth.

When machining with feed values significantly below h_{min}, material removal does not occur during the first pass of the cutting edge. At this stage, complex plastic deformation processes may take place. In the present study, it is assumed that the material does not undergo any state change: its properties remain constant, no ploughing occurs, and no chip formation takes place. Although cutting forces are observed in the model, material removal does not occur. The retained material is taken into account during the subsequent cutting edge pass, leading to an increase in the effective uncut chip thickness. For very small feed values, chip formation does not occur at this stage either, and the material from both the first and second cutting edge pass remains unremoved. Only when the minimum uncut chip thickness is exceeded in subsequent engagements does chip formation occur and the material is removed.

The described phenomenon explains the multiplication of the observed surface marks, whose spacing does not directly result from the feed per tooth value. **Figure 3** presents the surface marks observed experimentally, together with the modeled surface topography.

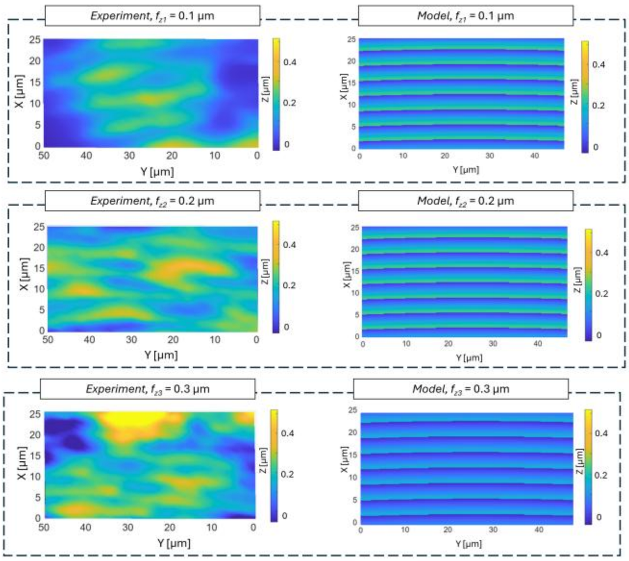

Figure 3. Experimental and modelled surface topographies

Although the accumulation mechanism was incorporated into the model, the size of the accumulation marks does not fully correspond to the size of the marks observed on the machined surface. This discrepancy results from plastic deformation effects that are not included in the model. Figure 4 presents the surface roughness of the experimentally observed surface and the modeled surface. In order to illustrate the influence of the accumulation mechanism, the results obtained using a model without the implemented accumulation mechanism are also included in the comparison. It is clearly visible that the incorporation of the accumulation mechanism leads to a significant improvement in the consistency between the surface roughness values.

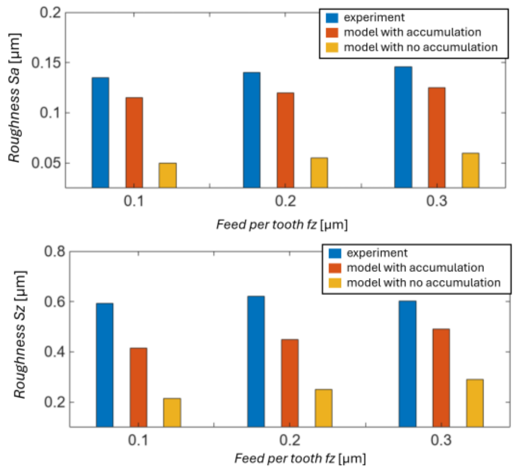

Figure 4. Roughness of experimental and modelled surfaces

3. Conclusion

This paper presents a micromachining model for end milling operations. The model accounts for both cutting forces and the resulting machined surface topography. In addition, the accumulation mechanism of the uncut chip layer is incorporated. The proposed model was validated through machining experiments conducted with feed per tooth values below the minimum uncut chip thickness. Based on the conducted study, the following conclusions can be drawn:

- The accumulation mechanism occurs when the nominal feed per tooth does not exceed the minimum uncut chip thickness.
- Incorporation of the accumulation mechanism makes it possible to obtain surface marks whose dimensions are larger than those resulting directly from the feed per tooth.
- Consideration of the accumulation mechanism improves the consistency between the experimentally obtained surface and the modeled surface.

Despite these improvements, full consistency between the modeled and experimental results was not achieved. The average relative error reached level of 14.5% for the surface roughness parameter Sa and 25.7% for Sz. In order to further improve the consistency, not only in terms of roughness parameters but also in reproducing accumulation marks, the plastic behavior of the machined material should be incorporated into the model.

References

[1] S. Wojciechowski, *Materials* **2021**, *15*, DOI 10.3390/ma15010059.

[2] D. Wang, J. Ren, W. Tian, *Int. J. Adv. Manuf. Technol.* **2020**, *107*, 2023.

[3] S. Wojciechowski, M. Wiackiewicz, G. M. Krolczyk, *Measurement* **2018**, *129*, 686.

[4] N. Grossi, A. Scippa, L. Sallese, F. Montevecchi, G. Campatelli, *Int. J. Mach. Tools Manuf.* **2018**, *133*, 31.

[5] K. J. Kalinski, M. A. Galewski, *Int. J. Mach. Tools Manuf.* **2015**, *92*, 19.

[6] G. Bissacco, H. N. Hansen, L. De Chiffre, *J. Mater. Process. Technol.* **2005**, *167*, 201.

[7] J. Chae, S. S. Park, T. Freiheit, *Int. J. Mach. Tools Manuf.* **2006**, *46*, 313.

[8] A. Simoneau, E. Ng, M. A. Elbestawi, *Int. J. Mach. Tools Manuf.* **2006**, *46*, 467.

[9] S. Wojciechowski, M. Matuszak, B. Powałka, M. Madajewski, R. W. Maruda, G. M. Królczyk, *Int. J. Mach. Tools Manuf.* **2019**, *147*, 103466.

[10] M. Gołaszewski, S. Wojciechowski, B. Powałka, F. Botko, M. Geľatko, *Precis. Eng.* **2026**, *97*, 904.